IEEE Access
Multidisciplinary | Rapid Review | Open Access Journal

Received May 16, 2021, accepted July 27, 2021, date of publication August 9, 2021, date of current version August 16, 2021.

Digital Object Identifier 10.1109/ACCESS.2021.3103202

Design and Control of an Omni-Directional Robotic Walker Based on Human–Machine Interaction

JIANCHENG JI[1,2], (Student Member, IEEE), WEI CHEN[1], WENBIN WANG[1], AND JASON XI[3]
[1]Institute of Intelligent Manufacturing Technology, Shenzhen Polytechnic, Shenzhen 518055, China
[2]Shenzhen Institutes of Advanced Technology, Chinese Academy of Sciences, Shenzhen 518055, China
[3]Department of Physical Therapy, Faculty of Medicine, University of Toronto, Toronto, ON M5G 1V7, Canada

Corresponding author: Wei Chen (chenweil@szpt.edu.cn)

This work was supported by the Key Project of Science and Technology of Guangdong Education Department under Grant 6020210086K.

This work involved human subjects or animals in its research. The authors confirm that all human/animal subject research procedures and protocols are exempt from review board approval.

ABSTRACT A cornerstone of the rehabilitative regime for people diagnosed with dyskinesia is walking assist and gait training, however, prolonged care, provided by relatives or professionals, serves as a massive financial burden to patients. The proposed novel robotic walker seeks to address this concern. The walker incorporates human motion intention recognition to facilitate lower limb rehabilitation training and daily walking. The walker design places strong emphasis on patient safety and quality of life by providing omni-directional walking assist, four key pelvic motions that support hip rotations and comfortable body weight support (BWS). Additionally, five sensors were installed to identify the user's motion intention from the interaction forces surrounding the pelvis and dead zone. Furthermore, Kalman filtering was used to guarantee the quality of the interactive signal while kinematic and dynamic models were derived to generate appropriate driving velocities to support patient's body weight and improve mobility. To validate our design, the MATLAB simulations and exploratory clinical trials using healthy subjects were performed. Preliminary results demonstrate satisfactory kinematic performance and suggest the walker as a promising therapeutic avenue for individuals suffering from dyskinesia and other associated movement disorders.

INDEX TERMS Lower rehabilitation robot, motion control, design, stroke, robotic walker, human–machine interaction.

I. INTRODUCTION

According to the World Health Organization, globally every year 15 million individuals suffer from a stroke and 33 million individuals present with some form of physical disability [1]. These prevalence levels present as a major rehabilitative challenge. Fueling this rise is an aging global population [2]. Increased age is linked with dysbasia and increased risk of falling. This is extremely worrisome as age serves as a major risk fact for dysbasia and increased risk of falling [3]. To combat this rise, rehabilitative regimes, comprising of healthcare professionals and their respective tools, have been established [4]. These regimes are crucial to preventing muscle atrophy and adhesion in individuals diagnosed with dysbasia [5]. However, a major limitation of the current method is the financial burden placed on the patient and the healthcare system, but community-based rehabilitation is the major method to improve gait function and minimize functional deficits for subsequent treatments. Taken together, it is evident that stroke and disability rehabilitation is essential, however, a more fiscally responsible method is required.

Mobility aids are important and have been developed to improve mobility and independent Activities of Daily (ADL) [8]. Today, a wide range of aids are implemented, from ultrasonic canes [6] to passive and active walkers [7]. Considering their constitutive materials, control methods and structural configurations, mobility aids can be divided into five major categories: electrically powered wheelchair, exoskeleton robot, intelligent ultrasonic cane, robot assist walker and robotic smart walker [9]. With respect to currently available walkers, the conventional design, constructed using casters and hand brakes [10], are easiest to manipulate, but much less effective in preventing falls and improving health outcomes compared to other designs such as walkers with electronic components and robotic smart walkers [11].

The associate editor coordinating the review of this manuscript and approving it for publication was Luigi Biagiotti.

Robotic walkers with electronic components, such as the passive i-Walker proposed by Cortes *et al.* [12] have emerged as an improved alternative for walking assistance. This type of walker controls the automated braking system while walking over ground [13]–[15]. Alternatively, robotic smart walkers with the BWS are developed to reduce the risks of training and accommodate for lack of physical support, the Andago robot of the Hocoma robotic device [16], provides users with continuous BWS. Based on clinical suggestions of using a mobility aid [17], the walker should maintain the stability of the center of mass (CoM), and provide patients with body support to facilitate the standing and walking well. Currently, the literature surrounding human-following is mainly focused on following the user's CoM and obstacle avoidance.

In order to better satisfy the clinical demands of the community at large, research regarding mobility aids has been focused towards automation, multi-function, and pelvic motions during the rehab process now. At present, the walkers are usually capable of identification of user's motion intention by sensors [18]–[20], In general, the human motion intention recognition tasks of a mobile aid could be divided into three steps: 1) Human detection via sensors, such as mechanical sensors and optical sensors; 2) Interactive signal processing; 3) Human motion state/intention estimation. For instance, the active robotic walker JARoW developed by Japan Advanced Institute of Science and Technology fulfills the functionalities of man-machine interaction via two infrared sensors, and estimate the walking state via the observation of shin distance [21]. To realize natural gait, pelvic motion module has been designed, such as the balance assessment robot (BAR) can control the haptic interaction by two force sensors, four servo motors and two spherical hinges [22]. The robotic walker developed by the National University of Singapore [23], can detect force and torque on the walker via a six-axis force/torque sensor, and then estimate the motion intention for over-ground walking.

The last step of walker control is to determine the velocity and direction of the platform, admittance control system is adopted extensively, such as the BAR implemented admittance-based haptic interaction control to satisfy the forces between the subject's pelvis and robot [24]. The DZ and the KF [25] are also widely applied in man-machine interactive control with excellent performance in reducing the effects of noise and interference from measurements effectively. Of particular note is that the existing interaction control and human following still existed several problems, such as the delay setting of the controller and accurate intention recognition, to solve the aforementioned challenges, key issues are as follows: 1) Reasonable setting of delay between the user's motion and actuators of the walker, for the instability of interactive signal caused by the irrelevant motions; 2) Obtaining the motion intention via sufficient sensors and reliable recognition algorithm. In this paper, we employ springs and cushion to reduce the noise of the interactive signal, and the DZ and the KF are applied to optimize the intention recognition. Ensuring both high accuracy and quick responsiveness, the velocity control method is proposed to achieve human-following tasks and feedforward control method is implemented to realize the accurate BWS. The main contributions of this paper are summarized as follows:

a) satisfied four key pelvic motions and covered the workspace;

b) designed a motorized walker with intention recognize system based on the mechanical sensors;

c) proposed a velocity control method and a feedforward control method to facilitate the human following and interaction control.

The presentation of this work is divided into five sections. In Sec. 2, the key pelvic motions are introduced, the conceptual design and recognition algorithm are detailed. Then, the kinematics of mobile platform and dynamics of the BWS system are studied in Sec. 3. Performance analysis and experimental studies are studied to demonstrate the effectiveness of the proposed system and methods in Sec. 4. Finally, conclusion and further developments of this work are given in Sec. 5.

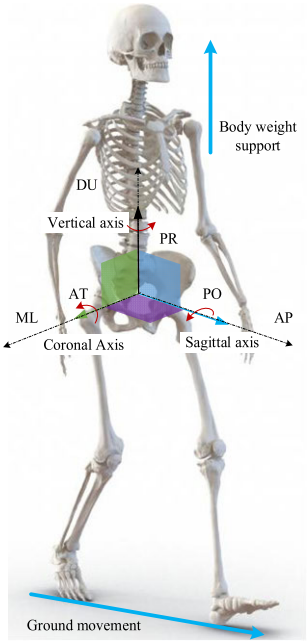

FIGURE 1. Schematic diagram of the pelvic motions.

II. SYSTEM DESCRIPTION

This chapter describes the mechanical structure of the omni-directional robotic walker (ORW), which is based on clinical need, and the recognition algorithm, which is based on mechanical sensors. The bilateral hip joints of the human pelvis, as shown in Fig 1, are the most complicated weight bearing structures in the body. Pelvic motions play an extremely importance role in walking and balance [26]. The human pelvis shows six basic movements in normal

walking, i.e., mediolateral motion (ML), anterior-posterior motion (AP), down-up motion (DU), anterior-posterior tilt (AT), pelvic obliquity (PO) and pelvic rotation (PR) [27]. Watanabe *et al.* [28] concluded that the ML, DU, PO and PR are key gait parameters, and are important for energy transformation and the maintenance of body stability. According to previous work, the estimated range of motion (RoM) of the pelvis during normal walking is given [29]. In addition, it is worth noting that the RoM of pelvis can vary greatly among different persons.

Although the literature has indicated that the previously mentioned four key motions are the dominant actions in balance training and gait rehabilitation, exercises which involve the AP and AT are still included in treadmill training and core muscle training. And the synchronized movement of pelvis is the basis of natural gait, which is more beneficial for motor relearning [30]. Furthermore, accounting for the six basic movements allows for more complex trajectories that are helpful for rehabilitation exercise. Therefore, designing a robotic walker that satisfies the pelvic motion requirements and has body weight support system is our objective.

A. SYSTEM DESCRIPTION

From the pelvic motion analysis and previous experience [31], it is difficult to achieve all pelvic motions and limit the RoM at the same time with serial mechanism. Having previously designed a walker with a serial pelvic mechanism, a major limitation was irregular signal inputs. On the contrary, parallel mechanisms are more likely to match the rotation axes and limit the RoM of pelvis than serial mechanisms. However, parallel mechanisms also present with limitations. For example, a small workspace and kinematic coupling. Therefore, a series-parallel mechanism was used to ensure all pelvic motions were satisfied, as shown in Fig. 2(b). In addition, the mounting position of wheels were altered to enhance the dexterity of the walker, and it has an edge in narrow space.

A robotic walker prototype was developed with a healthy volunteer as shown in Fig. 2(a), the ORW consists of three main parts: i) an omni-directional mobile platform (OMP); ii) a body weight support system (BWSS) and iii) a pelvic brace (PB) with mechanical sensors. The purpose of the OMP is to provide omni-directional over-ground mobility. It is designed as a ring-shaped rigid steel frame. Once the electrical components are installed, the patient has 0.4 m of free space in the ML direction, and 1.2 m of free space in the AP direction. The OMP is supported with three omni-directional wheels and two passive caster wheels to maintain the stability. The omni-directional wheels are mounted underneath the frame with three 10:1 gear reduction unit (T.W.T Co., Ltd. TR 60) and three servo motors of the Beckhoff Co., Ltd. AM8122, to achieve over-ground move with respect to the pelvic center.

The purpose of the BWSS is to provide body weight support during gait and achieve the sit-to-stand (STS) transfer. The BWSS can achieve a vertical displacement of 0.5 m for body weight support via a parallel four-bar mechanism, the trajectory of end is semi-circular shaped while the pose is unaltered. The BWSS is actuated by a servo motor of the Beckhoff Co., Ltd. AM8131 with a 120:1 gear reduction unit (T.W.T Co., Ltd. TR 90). Additionally, ten tension springs are mounted between the two parallel bars,

(a)

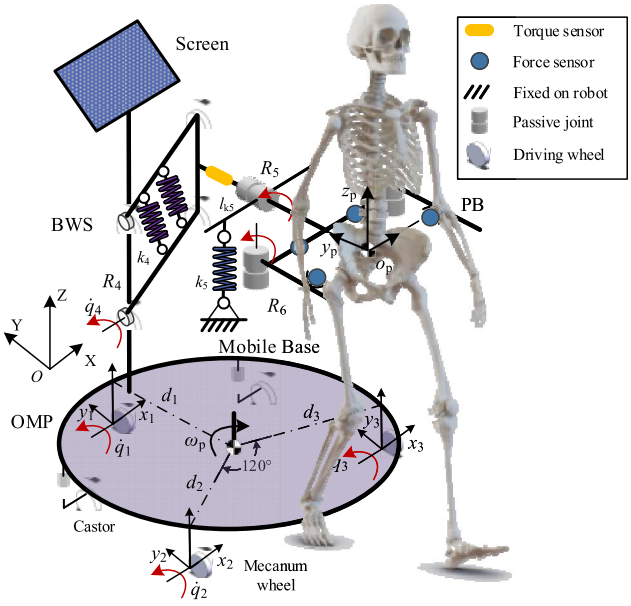

(b)

FIGURE 2. Prototype and schematic diagram of the ORW. The OMP represents the omni-directional mobile platform, the BWSS represents the body weight support system and the PB represents the pelvic brace.

to relieve the load of the motor. And a laptop PC (Surface Pro 7) that runs on Microsoft's Windows 10 as the upper computer on top of the BWSS frame.

The PB is designed to be installed on the end of the BWSS, a torque sensor (SBT851/±500 N·m) is mounted between the PB and the BWSS. It is of three degrees-of-freedom (DoFs) to achieve natural pelvic motions. The first DoF (R_5) is realized by a rotary joint which is parallel to ground, it allows the pelvic obliquity of ±10 ° with two compressed springs to provide reset force. And its axis passes through the pelvic center like the wrist joint of industrial robot [32], hence it will not lead to displacement of the pelvis. The last DoF is realized by a parallel four-bar mechanism, two ball splines and user's pelvis, the pelvis can rotate around the Z axis, the RoM is ±10 °; and this mechanism allows the ML move of ±25 mm. Four pressure sensors (SBT741/±20 kg) are installed around the pelvis to identify the user's motion intention, and a safety belt is employed to connect the walker.

While the OMP and the BWS are driven by actuators, the PB is completely passive with flexibility. All joint flexibility is realized by springs, as shown in Fig. 2. The primary function of springs is to maintain pelvis in the balance position and orientation, the force value of 30-50 N is enough to guide the pelvic motions. However, researchers suggest that the force value of 80-120 N is eligible to change the balanced state [33], [34]. Therefore, the design of spring stiffness is based on the interaction force and RoM of pelvis in this paper. During walking with the walker, the subject is connected to ORW through a harness, and the subject can manipulate the walker via pelvic motions. Four pressure sensors and one torque sensor are installed at the connection points around the pelvis to measure the interaction force. The main power supply consists of two 48 V, 12 Ah lithium batteries that power the motor drivers, laptop PC and controller. The data collection, signal processing and velocity control are done on the Beckhoff PLC CX-5130 embedded PC in TwinCAT2.

B. RECOGNITION ALGORITHM

As the walker is designed to assist patients with walking and weight lifting, an intention-based recognition algorithm is designed to detect the interaction forces and moments, as shown in Fig. 3. During the operation of the walker, the user first applies forces and moments on the force and torque sensors. These signals are then sent to the intention-based controller to determine the corresponding walking intention. With the user's intention and motion states of the walker, the controller will generate proper motor speeds to assist the user for maneuver. The human pelvis connects the robot via two spherical hinges and the harness. When the pelvis moves or rotates, pelvis presses the four force sensors and torque sensor, then the sensors connected with the walker will generate force signal f_i(i = 1,2,3,4) and torque sensor will generate torque signal t_5. The distance from the axis of R_5 to the axis of the front force sensors is u_i(i = 1,2). The distance

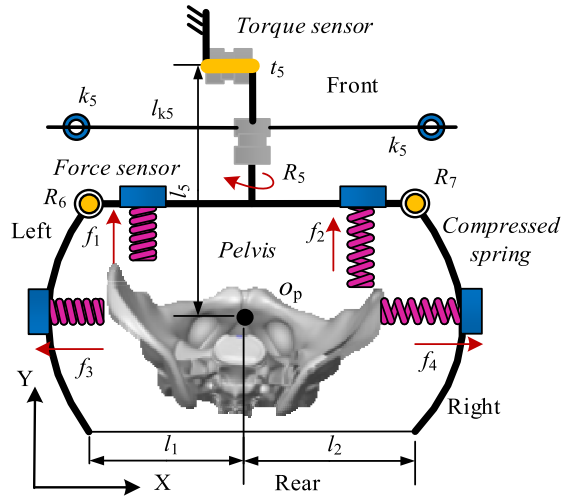

FIGURE 3. Foundation of intention recognition controller.

from the axis of torque sensor to the pelvic center is l_5. Then the resultant force/moment is defined as:

$$\begin{cases} F_x = \sum f_i & (i = 3, 4) \\ F_y = \sum f_i & (i = 1, 2) \\ F_z = t_5/l_5 & \\ M_z = \sum (f_i \times u_i) & (i = 1, 2) \end{cases} \tag{1}$$

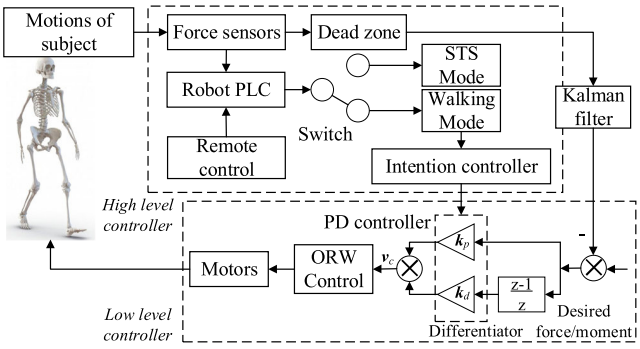

FIGURE 4. Control architecture of the robotic walker.

The resultant forces and torques are then used to implement an intention control with the control flow chart given in Fig. 4, The control system should have robustness to ignore normal oscillations in the signals that result from walking and sensor noise, dead zone and Kalman filtering are used to guarantee the quality of interactive signal. We defined two threshold values (TV): F_t is the threshold value for rectilinear motion, and M_t is the threshold value for curvilinear motion, and its value is determined by trial and error. Overlarge threshold value will cause vibration and tiny threshold value is not beneficial to stability. Then the control algorithm is defined, as shown in Table 1: 1) if $F_y > F_t$, $|M_z| < M_t$ and $|F_x| < F_t$, then move forward; 2) if $F_x < -F_t$, $|M_z| < M_t$ and

TABLE 1. Basic motion patterns with respect to force/moment signals.

	f_1	f_2	f_3	f_4	t_5
Forward	>TV	>TV	||<TV	||<TV	\
Left	||<TV	||<TV	>TV	||<TV	\
Right	||<TV	||<TV	||<TV	>TV	\
Turn left	(f_2>f_1) & |f_2-f_1|>TV		||<TV	||<TV	\
Turn right	(f_1>f_2) & |f_1-f_2|>TV		||<TV	||<TV	\
Up	\	\	\	\	>TV
Down	\	\	\	\	<-TV
Halt	ELSE				

TV means threshold value and || means absolute value.

$|F_y| < F_t$, then move to left; 3) if $F_x > F_t$, $|M_z| < M_t$ and $|F_y| < F_t$, then move to right; 4) if $M_z > M_t$ and $|F_y| < F_t$, then turn left; 5) if $M_z < -M_t$ and $|F_y| < F_t$, then turn right; 6), and if other conditions, then stop. For the intention controller of the BWSS, the executes control as follows: 1) if $F_z > F_t$, then move upward; 2) if $F_z < -F_t$, then move downward; 3) and if other conditions, then stop.

C. CONTROL ARCHITECTURE

The input and output of the closed-loop control system are interaction forces/torques and actuating speed of motors, as shown in Fig. 4, the first step is that the sensors measure the error between the interaction forces/torques and desire forces/torques, then the PLC calculates the actuating speed of motors, the intention controller is to choose the PD controller parameters based on the motion state and force/torque signals. The users can switch the move mode via the remote control, and dead zone and the KF were applied to reduce the effects of noise and interference. The low-level controller is executed at 1000 Hz and the high-level controller is executed at 100 Hz. During walking with the walker, the PLC reads the force/moment signals generated by the pelvis motion, and then the intention controller determines the corresponding walking intention and controls the motor velocity to assist the user in walking and standing.

Affected by the composition error and zero drift of the sensors, and irrelevant motions and instability of the CoM, the motion control of the walker is challengeable. Therefore, the KF was enforced to relieve the aforementioned interference, the estimation and correction process can be expressed as:

$$\boldsymbol{x}_t = \boldsymbol{A}\boldsymbol{x}_{t-1} + \boldsymbol{K}_t\left(z_t - \boldsymbol{C}\boldsymbol{A}\boldsymbol{x}_{t-1}\right) \tag{2}$$

where

$$\boldsymbol{K}_t = \boldsymbol{P}_t\boldsymbol{C}^T\left(\boldsymbol{C}\boldsymbol{P}_t\boldsymbol{C}^T + \boldsymbol{R}\right)^{-1} \tag{3}$$

$$\boldsymbol{P}_t = \boldsymbol{A}\boldsymbol{P}_{t-1}\boldsymbol{A}^T + \boldsymbol{Q} \tag{4}$$

$$z_t = \begin{bmatrix} f_1 & f_2 & f_3 & f_4 & t_5 \end{bmatrix}^T \tag{5}$$

$\boldsymbol{x_t}$ represents the real state of the system at moment t, $\boldsymbol{A}$ represents the state-transition matrix, $\boldsymbol{K_t}$ is the Kalman gain at moment t, $z_t = \begin{bmatrix} \boldsymbol{f_1} & \boldsymbol{f_2} & \boldsymbol{f_3} & \boldsymbol{f_4} & \boldsymbol{t_5} \end{bmatrix}^T$ represents the observed value matrix at moment t, $\boldsymbol{C}$ is measurement matrix, $\boldsymbol{P_t}$ is the error matrix at moment t, $\boldsymbol{R}$ is the covariance matrix of measurement noise, $\boldsymbol{Q}$ is the covariance matrix of predicted noise.

We can achieve the aforementioned motion modes via velocity of the OMP, angular velocity of the OMP and velocity of the BWSS, so the relation between input force/moment and output velocity can be expressed as:

$$\boldsymbol{v}_c = \boldsymbol{k}_\tau\boldsymbol{\tau}_c + \boldsymbol{k}_p\boldsymbol{f}_e + \boldsymbol{k}_d\dot{\boldsymbol{f}}_e \tag{6}$$

where $\boldsymbol{v}_c = \begin{bmatrix} \dot{x}_c & \dot{y}_c & \dot{z}_c & \omega_c \end{bmatrix}^T$ is the theoretical output velocity of the robotic walker, $\boldsymbol{f}_e$ is the tracking error between the resultant wrench $\boldsymbol{F}_s = \begin{bmatrix} F_x & F_y & F_z & M_z \end{bmatrix}^T$ and the required wrench $\boldsymbol{F}_r = \begin{bmatrix} F_{xr} & F_{yr} & F_{zr} & M_{zr} \end{bmatrix}^T$, $\dot{\boldsymbol{f}}_e$ is the differential error, $\boldsymbol{k}_p$ and $\boldsymbol{k}_p$ are the PD parameters of the control algorithm, $\boldsymbol{\tau}_c$ is the computed torque and $\boldsymbol{k}_\tau$ is the gain coefficient to involve the generalized mass and viscous friction in the controller to eliminate the delay. To calculate the output velocity of each motor of the walker, kinematical and dynamics modeling are required.

III. DYNAMICS MODELING

Figure 2 is a kinematic model of the walker, depicting the motion principle of each joint. In kinematic modeling, the kinematical equations of the active joints were derivated via a vectorial method in this paper. The derivation process of the kinetic equation is presented, as shown in Fig. 5, form the tip to the actuating shaft.

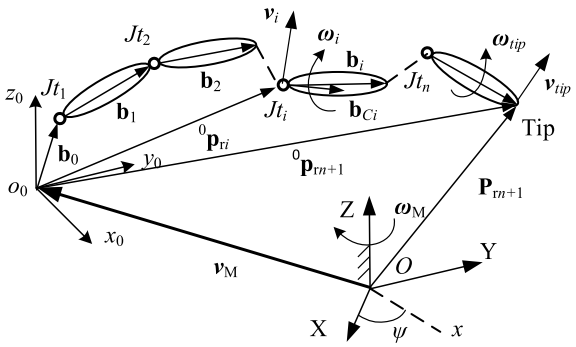

FIGURE 5. Kinetic reaction in multi-rigid-body system.

A. KINEMATICS OF THE WALKER

The patient's pelvis is considered as the end-effector defined by a body coordinate frame $O_pX_pY_pZ_p$ is attached, with origin O_p at the center of the pelvis. The initial orientation of the body coordinate frame is aligned with the fixed coordinate frame. The Vector $\boldsymbol{P}$ expresses the position from O_0 to O_b. The Matrix $\boldsymbol{R}$ describes the rotation from the body frame to the fixed frame, and α denotes the angle of the rotation around the X axis (X Euler angle signifies pelvic tilt); β is the angle around Y axis (Y Euler angle signifies pelvic

obliquity); γ is the angle around Z axis (Z Euler angle signifies pelvic rotation).

The OXYZ is set as a global coordinate system with the origin at a point in space. $o_0x_0y_0z_0$ is the local coordinate system attached to the OMP and its position and orientation is defined as $\boldsymbol{p}_{\mathrm{M}} = [x\ y\ 0]^T$ and $\boldsymbol{o}_{\mathrm{M}} = [0\ 0\ \Psi]^T$. The twist of the OMP in the OXYZ frame is expressed as $\boldsymbol{t}_{\mathrm{M}} = [\boldsymbol{v}_{\mathrm{M}}\ \boldsymbol{\omega}_{\mathrm{M}}]^T$, and in the local coordinate frame as $\boldsymbol{t}_R = [\boldsymbol{v}_R\ \boldsymbol{\omega}_R]^T$. For the walker, r denotes the radius of driving wheel; d_i denotes the distance between o_{pp} (projection of o_p) and each wheel position; φ_i denotes the angular displacement of the ith wheel; R denotes the radius of the platform; and point C is the mass center of the mobile platform. The rotation speeds of the three driving wheels are defined as $\boldsymbol{\omega}_w = [\dot{q}_1\ \dot{q}_2\ \dot{q}_3]^T$. Under the assumption of pure rolling without slippage, the kinematic equation of the OMP can be expressed:

$$\boldsymbol{\omega}_w = \mathbf{J}_{\boldsymbol{w}}^{-1}\boldsymbol{t}_R \tag{7}$$

where

$$\mathbf{J}_{\boldsymbol{w}}^{-1} = \frac{1}{r}\begin{bmatrix} -1 & 0 & 0 & 0 & 0 & d_1\cos(\pi/2-\varphi_1) \\ 0.5 & -0.866 & 0 & 0 & 0 & d_2\cos(\pi/6-\varphi_2) \\ 0.5 & 0.866 & 0 & 0 & 0 & d_3\cos(\pi/6+\varphi_3) \end{bmatrix} \tag{8}$$

$$d_i = \sqrt{(y_i - y_p)^2 + (x_i - x_p)^2} \tag{9}$$

$$\varphi_i = \tan^{-1}\left(\frac{y_i - y_p}{x_i - x_p}\right) \tag{10}$$

$$y_p = l_5 + \sin q_4 l_4 \tag{11}$$

where (x_i, y_i) is the position coordinate of ith wheel on the ground, and (x_p, y_p) is the projected coordinate of pelvic center in the horizontal plane. y_p is influenced by the motion of the BWSS system while x_p is unaltered. Combining Eq. (6) and Eq. (7), we can control the motors of the OMP. Then the $\boldsymbol{t}_{\mathrm{M}}$ can be obtained by multiplying a rotation matrix.

According to the Fig. 2, the position vector from the global origin to the ith joint can be expressed as:

$$\boldsymbol{P}_i = \boldsymbol{p}_{\mathrm{M}} + \boldsymbol{l}_0 + \sum_{j=4}^{i} \boldsymbol{R}_j \boldsymbol{P}'_j \tag{12}$$

Taking derivative of Eq. (12) yields the linear velocity vector as

$$\dot{\boldsymbol{P}}_i = \boldsymbol{v}_{\mathrm{M}} + \boldsymbol{\omega}_{\mathrm{M}} \times \boldsymbol{l}_0 + \sum_{i=j}^{i} \boldsymbol{\omega}_j^G \times \boldsymbol{R}_j \boldsymbol{P}'_j \tag{13}$$

where $\boldsymbol{\omega}_j^G$ is the body angular velocity vector expressed as

$$\boldsymbol{\omega}_j^G = \boldsymbol{\omega}_{\mathrm{M}} + \sum_{k=4}^{j} \dot{q}_k \dot{\boldsymbol{z}}_k \tag{14}$$

where $\dot{q}_k (k = 4, 5, 6, 7)$ is the kth joint velocity, $\dot{z}_k$ is the kth joint unit vector of rotation axis. Substituting equation (14) into (13) yields twist vector of the ith joint in the global frame:

$${}^W\boldsymbol{v}_i = {}^W\boldsymbol{v}_{\mathrm{M}} + {}^W\boldsymbol{\omega}_{\mathrm{M}} \times \boldsymbol{b}_0 + \sum_{j=1}^{i} \boldsymbol{\omega}_j^w \times \left({}^1\boldsymbol{R}_j \boldsymbol{b}'_j\right) \tag{15}$$

$${}^W\boldsymbol{\omega}_i = {}^W\boldsymbol{\omega}_{\mathrm{M}} + \sum_{j=1}^{i} \dot{q}_j \boldsymbol{z}_j \tag{16}$$

Taking derivative of Eq. (15) and (16) yields the acceleration twist as:

$$\begin{aligned} {}^W\dot{\boldsymbol{v}}_i = {}^W\dot{\boldsymbol{v}}_{\mathrm{M}} + {}^W\dot{\boldsymbol{\omega}}_{\mathrm{M}} \times \boldsymbol{b}_0 + {}^W\boldsymbol{\omega}_{\mathrm{M}} \times \left({}^W\boldsymbol{\omega}_{\mathrm{M}} \times \boldsymbol{b}_0\right) \\ + \sum_{j=1}^{i} \dot{\boldsymbol{\omega}}_j^w \times \left({}^1\boldsymbol{R}_{rj}\boldsymbol{b}'_j\right) + \sum_{j=1}^{i} \boldsymbol{\omega}_j^w \\ \times \left(\boldsymbol{\omega}_j^w \times \left({}^1\boldsymbol{R}_j \boldsymbol{b}'_j\right)\right) \end{aligned} \tag{17}$$

$${}^W\dot{\boldsymbol{\omega}}_i = {}^W\dot{\boldsymbol{\omega}}_{\mathrm{M}} + \sum_{j=1}^{i} \ddot{q}_j \boldsymbol{z}_j + {}^W\boldsymbol{\omega}_{ri} \times \left(\sum_{j=1}^{i} \dot{q}_j \boldsymbol{z}_j\right) \tag{18}$$

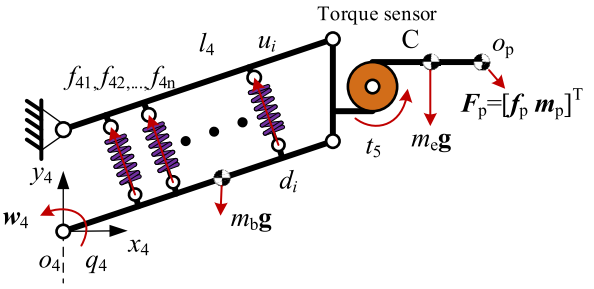

FIGURE 6. Forces and moments on the BWSS.

B. DYNAMICS OF THE WALKER

For the joints 5∼7 have tiny effect on the control, this section focuses on the dynamics of joint 4, as shown in Fig. 6, the tip wrench acted on the end of the walker, and the torque sensor monitored the vertical component of the wrench and part gravity of the PB. The actuating shaft should conquer the equivalent torque generated by the wrench, inertia force, elastic force and gyroscopic couple.

For the elastic force, in the joint coordinate system, the point d_i denotes the lower connection point of the tension spring, and u_i denotes the upper connection point. Then the equivalent resultant moment can be expressed:

$$\tau_{4t} = \sum (\boldsymbol{f}_{4i} \times \boldsymbol{l}_{4i})(i = 1, 2, \ldots, n) \tag{19}$$

where

$$\boldsymbol{f}_{4i} = f_{4i} \cdot \left(\overrightarrow{u_i d_i}\,|u_i d_i|\right) \tag{20}$$

$$\boldsymbol{l}_{4i} = [x_{di}\quad y_{di}\quad 0]^T \tag{21}$$

$$f_{4i} = k_4 (l_{ai} - l_o) \tag{22}$$

$$l_{ai} = \sqrt{(x_{ui} - x_{di})^2 + (y_{ui} - y_{di})^2} \tag{23}$$

where (x_{ui}, y_{ui}) is the position coordinate of ith connection point, l_o is the original length of the tension spring, k_4 is the elastic coefficient, and n is the number of tension springs.

Using a backward recursive method, the wrench acting on the ith joint can be expressed as:

$$\boldsymbol{w}_i = \mathbf{M}_i \dot{\boldsymbol{t}}_i^J + \mathbf{B}_i + \mathbf{H}_{ii+1}\mathbf{w}_{i+1} \tag{24}$$

where $\mathbf{w}_i = [\mathbf{f}_i^J\ \mathbf{m}_i^J]^T$ is the wrench including force vector $\mathbf{f}_i^J$ and moment vector $\mathbf{m}_i^J$ of ith joint, $\mathbf{M}_i$ is the generalized mass matrix, $\dot{\boldsymbol{t}}_i^J$ is the vector including linear acceleration

vector $\mathbf{a}_i - \mathbf{g}$ and angular acceleration vector $\boldsymbol{\alpha}_i$, $\mathbf{B}_i$ is the matrix including centrifugal forces and gyroscopic moments, $\mathbf{w}_{i+1} = \left[\mathbf{f}_{i+1}^J \ \mathbf{m}_{i+1}^J\right]^T$ is the wrench of $(i+1)$th joint or external wrench, $\mathbf{H}_{ii+1}$ is the transformation matrix. The segment angular velocity and acceleration $(\boldsymbol{\omega}_i, \boldsymbol{\alpha}_i)$ and linear acceleration of centre of mass $(\boldsymbol{a}_i)$ had been calculated via kinematics and derivation. Then the wrench of joint 4 can be expressed as:

$$\begin{aligned} \boldsymbol{w}_4 = &\sum_{j=4}^{7}\left[\prod_{i=4}^{j}\left(\mathbf{H}_{i-1,i}\right)\mathbf{M}_i\dot{\boldsymbol{t}}_i^J\right] \\ &+\sum_{j=4}^{7}\left[\prod_{i=4}^{j}\left(\mathbf{H}_{i-1,i}\right)\mathbf{B}_i\right]+\prod_{i=4}^{7}\left(\mathbf{H}_{i-1,i}\right)\boldsymbol{w}_{p7} \end{aligned} \tag{25}$$

where $\boldsymbol{w}_{p7} = \left[\boldsymbol{f}_p \ \boldsymbol{m}_p\right]^T$, and projecting $\boldsymbol{w}_4$ to the z_4 axis, we can obtain

$$\begin{aligned} \tau_{4c} = &\left(\mathrm{m}_4+\mathrm{m}_5+\cdots+\mathrm{m}_7\right)\left(l_4\ddot{q}_4\cos q_4-\mathrm{g}_z\right) \\ &+\underline{I}_{r4}\ddot{q}_4+\underline{I}_{r4}\dot{q}_4^2+f_{zt} \end{aligned} \tag{26}$$

where m_i is the mass of ith bar, $\underline{I}_{r4}$ is the simplified inertia, and f_{zt} is the vertical force calculated via the torque sensor. Then the output torque of the motor can be expressed as:

$$\tau_4 = \tau_{4c} - \tau_{4t} \tag{27}$$

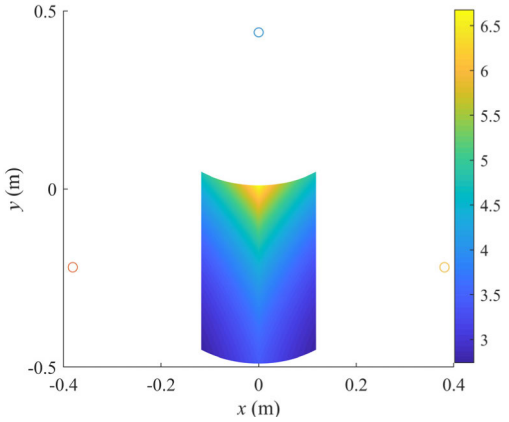

FIGURE 7. The color scale encodes the dexterity in the workspace; blue indicates areas with higher dexterity of the walker and three circles donate the three wheels.

IV. PERFORMANCE ANALYSIS

The workspace of the robotic walker was analyzed during the processes of the STS transfer and over-ground walking in [32]. This paper focused on the analysis of dexterity, effectiveness and maneuverability.

A. SIMULATION STUDY

The dexterity of the robotic walker was discussed by way of ascertaining the indices of the condition number of the Jacobian matrix to evaluate the kinematic performance of the walker. The Jacobian matrix $\mathbf{J}$ of the system can be calculated by the kinematics. The condition number was calculated as:

$$\kappa\left(\mathbf{J}\right) = \|\mathbf{J}\|\left\|\mathbf{J}^{-1}\right\| \tag{28}$$

The simulation results show that the walker had a large workspace and it's completely symmetric about the y-axis. The maximal condition number (6.7) appears at the middle-upper part of reachable workspace, the minimal dexterity index is 2.8. When reachable point closes to the center of the walker, the dexterity index declines to 6.7 and the reachable pose is decreasing. The simulation results indicate that the reachable workspace of walker can cover the desired motion space of pelvis, and no dramatic change of condition number demonstrates that the dexterity of the robotic walker is satisfactory.

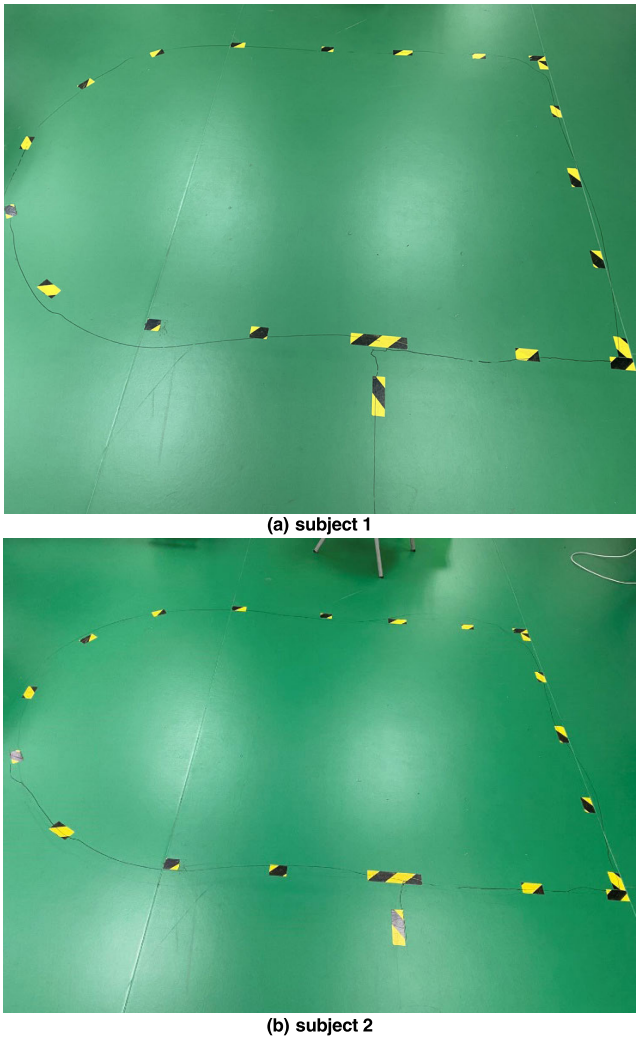

(a) subject 1

(b) subject 2

FIGURE 8. Verification experiment with subject 1 (a) and subject 2 (b). The attention line is the reference path and the black line represents the actual path.

B. EXPERIMENTAL STUDIES

In this section, two experiments were carried out to assess the following and unloading force performance of the walker. Firstly, two volunteers were asked to walk along a given path. The path is designed as a foursquare curve with a semicircle line, as shown in Fig. 8, in order to challenge the individual to use all moving modes. The task is extremely challenging for

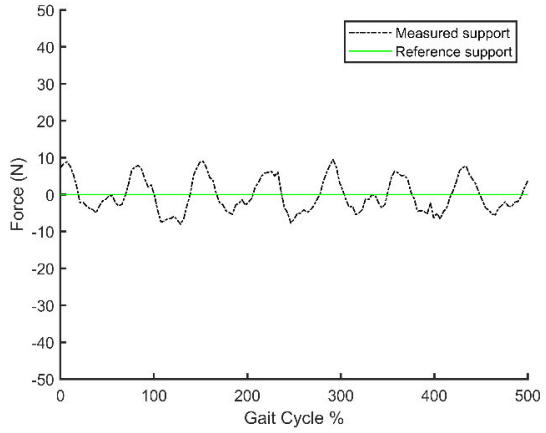

(a) subject 1 with unloading of 0 kg

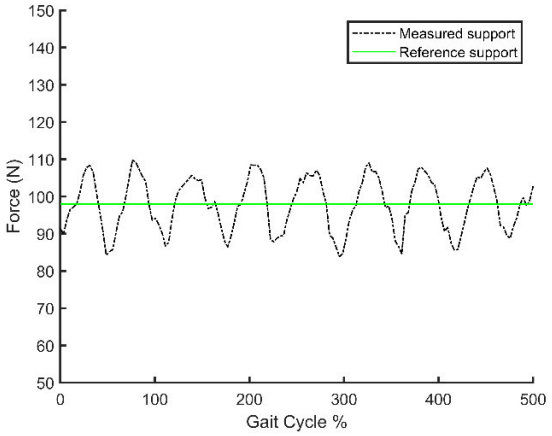

(b) subject 1 with unloading of 10 kg

FIGURE 9. Translated torque sensor signal with a reference support.

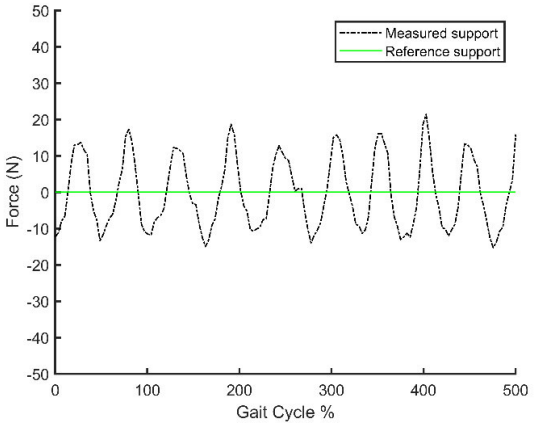

(a) subject 2 with unloading of 0 kg

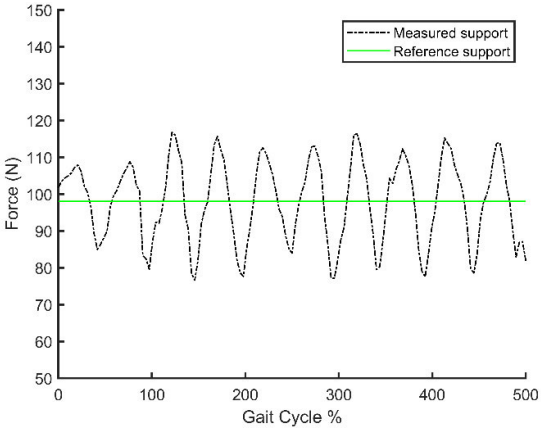

(b) subject 2 with unloading of 10 kg

FIGURE 10. Translated torque sensor signal with a reference support.

TABLE 2. Subject information.

Subject	Gender	Age (year)	Height (cm)	Weight (kg)
*S*1	Male	30	175	72
*S*2	Female	31	162	48

Inclusion criteria: no abnormalities in nervous system, muscle-bone system and physical examination; No special balance training previously.

the maneuverability of the ORW. Participants were instructed to follow the attention line indicated on the ground. Two trials were conducted for each participant and the experimental results were recorded by the black line. To record the black line, a marking pen was fixed to the front of the walker and was visible to the experimenters. As indicated in table 2, the average participant age, height and weight was 30.5m, 168.5 cm and 60.0 kg respectively. Each individual was anchored to the walker through a harness and was given a 5 min acclimation period before being instructed to complete the task within 30 seconds. The start point, end point and waypoint were also recorded.

The second experiment assessed unloading force performance. Individuals were instructed to walk using the walker while either a 0 kg or 10 kg was concurrently unloaded. The signal of the torque sensor and gait cycle (GC) were then measured. Two healthy adults were asked to walk at comfortable speed along a straight line, experimental data from the BWSS device were translated into the vertical force.

As seen in Figure 8(a∼b), which depicts the results from the first experiment, both participants were able to follow the given path within an acceptable error range. This indicates that the walker allowed the user to walk naturally under the controller and the proposed control methods were effective. This finding supports the feasibility of incorporating the walker into therapeutic regimes However, a limitation of the walker was user control. For example, as noted by study participants the walker could easily get out of hand at warp speed. This is further supported by figure 8(a), where, the walker is shown to deviate from the attention line in Fig. 8(a). To address this concern, joysticks will be added in the future.

The recorded data shown here are typical for the achieved unloading force performance, as shown in Fig. 9∼10.

The controller as described in the previous section was based on the PD controller and dynamic model with the unloading force. Furthermore, data is presented that was obtained with the two volunteers. The unloading performance can be described via the peak error, mean error and standard deviation. According to the results, for the subject 1 with unloading of 0 kg, the peak error was 9.5 N, mean error was 4.6 N and standard deviation was 3.4 N; for the subject 1 with unloading of 10 kg, the peak error was 16.6 N, mean error was 8.7 N and standard deviation was 6.5 N; for the subject 2 with unloading of 0 kg, the peak error was 21.4 N, mean error was 8.6 N and standard deviation was 4.8 N; for the subject 2 with unloading of 10 kg, the peak error was 26.4 N, mean error was 9.7 N and standard deviation was 5.8 N, which indicated the unloading force performance of the walker during the walking process. We may conclude that the walker is capable of body weight support for patients.

V. CONCLUSION

In this paper, a novel omni-directional robotic walker, along with the associated dynamic models and implemented control algorithm, was described in this paper. Effective design allows for the walker to be controlled by user pelvic motion. Furthermore, the proposed control methods, intention recognition and body weight support, were effective with middle-low walking speeds. Importantly, instead of solely providing a constant unloading force, the walker synchronously follows the user to ensure safety. Taken together, research findings support the feasibility of the walker to be included in therapeutic regimes implemented to improve gait function via natural walking. However, before the proposed walker becomes widely adopted, the limitations need to first be addressed. Future studies should focus on improving interaction forces and address torque control.

ACKNOWLEDGMENT

The statements made herein are solely the responsibility of the authors.

REFERENCES

[1] W. Johnson, O. Onuma, M. Owolabi, and S. Sachdev, "Stroke: A global response is needed," *Bull. World Health Org.*, vol. 94, no. 9, pp. 634A–635A, Sep. 2016.
[2] R. Allison, "Developing a longitudinal profile of the consequences of the profoundly-affected arm after stroke: A feasibility study," Ph.D. dissertation, College Med. Health, Univ. Exeter, Devon, U.K., 2013.
[3] F. Batchelor, K. Hill, S. Mackintosh, and C. Said, "What works in falls prevention after stroke?" *Stroke*, vol. 41, no. 8, pp. 1715–1722, Aug. 2010.
[4] M. Arnold, E. Roe, and D. Williams, "A pictorial overview of technology-assisted care options for bariatric patients: One hospital's experience," *Ostomy/Wound Manage.*, vol. 60, no. 1, pp. 36–42, Jan. 2014.
[5] I. Dovgiy and N. Svyrydova, "Rehabilitation of patients suffering from ischemic stroke by methods of ozonotherapy, kinesitherapy, physiotherapy and acupuncture," *East Eur. J. Neurol.*, vol. 6, no. 12, pp. 4–9, Dec. 2016.
[6] Q. Yan, J. Huang, Z. Yang, Y. Hasegawa, and T. M. F. T. Fukuda, "Human-following control of cane-type walking-aid robot within fixed relative posture," *IEEE/ASME Trans. Mechatronics*, early access, Mar. 23, 2021, doi: 10.1109/TMECH.2021.3068138.
[7] M. Martins, C. Santos, A. Frizera, and R. Ceres, "A review of the functionalities of smart Walkers," *Med. Eng. Phys.*, vol. 37, no. 10, pp. 917–928, Oct. 2015.
[8] U. R. Roentgen, G. J. Gelderblom, M. Soede, and L. P. De Witte, "Inventory of electronic mobility aids for persons with visual impairments: A literature review," *J. Vis. Impairment Blindness*, vol. 102, no. 11, pp. 702–723, Nov. 2008.
[9] M. M. Martins, C. P. Santos, A. Frizera-Neto, and R. Ceres, "Assistive mobility devices focusing on smart Walkers: Classification and review," *Robot. Auto. Syst.*, vol. 60, no. 4, pp. 548–562, Apr. 2012.
[10] D. Molloy. *Boomer: A User Friendly Walking Aid for Eldery People*. Accessed: Jul. 10, 2019. [Online]. Available: http://www.tuvie.com/boomer-a-user-friendly-walking-aid-for-eldery-people/
[11] O. Postolache, J. M. D. Pereira, V. Viegas, L. Pedro, P. S. Girão, R. Oliveira, and G. Postolache, "Smart walker solutions for physical rehabilitation," *IEEE Instrum. Meas. Mag.*, vol. 18, no. 5, pp. 21–30, Oct. 2015.
[12] U. Cortés, A. Martínez-Valesco, C. Barrué, T. Benedico, F. Campana, J. Fernandez, and R. Annichiarico, "A SHARE-it service to elders' mobility using the i-walker," *Gerontechnology*, vol. 7, no. 2, p. 95, Apr. 2008.
[13] Y.-H. Hsieh, K.-Y. Young, and C.-H. Ko, "Effective maneuver for passive robot walking helper based on user intention," *IEEE Trans. Ind. Electron.*, vol. 62, no. 10, pp. 6404–6416, Oct. 2015, doi: 10.1109/TIE.2015.2416679.
[14] Y. Hirata, A. Hara, and K. Kosuge, "Motion control of passive intelligent walker using servo brakes," *IEEE Trans. Robot.*, vol. 23, no. 5, pp. 981–990, Oct. 2007, doi: 10.1109/TRO.2007.906252.
[15] A. F. Neto, J. A. Gallego, E. Rocon, J. L. Pons, and R. Ceres, "Extraction of user's navigation commands from upper body force interaction in walker assisted gait," *Biomed. Eng. OnLine*, vol. 9, no. 1, pp. 1–16, Aug. 2010.
[16] H. Hedel, I. Rosselli, and S. Baumgartner-Ricklin, "Clinical utility of the over-ground bodyweight-supporting walking system Andago in children and youths with gait impairments," *J. Neuroeng. Rehabil.*, vol. 18, no. 1, pp. 18–29, Feb. 2021.
[17] A. J. C. Sadowski, "Ambulatory assistive devices: How to appropriately measure and safely use canes, crutches and walkers," *Pharmacy Pract.*, vol. 1, no. 10, pp. 24–31, 2014.
[18] D. Schulz, W. Burgard, D. Fox, and A. B. Cremers, "People tracking with mobile robots using sample-based joint probabilistic data association filters," *Int. J. Robot. Res.*, vol. 22, no. 2, pp. 99–116, 2003.
[19] J. Huang, W. Huo, W. Xu, S. Mohammed, and Y. Amirat, "Control of upper-limb power-assist exoskeleton using a human-robot interface based on motion intention recognition," *IEEE Trans. Autom. Sci. Eng.*, vol. 12, no. 4, pp. 1257–1270, Oct. 2015, doi: 10.1109/TASE.2015.2466634.
[20] T. M. Gambon, J. P. Schmiedeler, and P. M. Wensing, "Effects of user intent changes on onboard sensor measurements during exoskeleton-assisted walking," *IEEE Access*, vol. 8, pp. 224071–224082, 2020, doi: 10.1109/ACCESS.2020.3044255.
[21] G. Lee, T. Ohnuma, N. Y. Chong, and S. Lee, "Walking intent-based movement control for JAIST active robotic walker," *IEEE Trans. Syst., Man, Cybern., Syst.*, vol. 44, no. 5, pp. 665–672, May 2014, doi: 10.1109/TSMC.2013.2270225.
[22] A. Olensek, M. Zadravec, and Z. Matjacic, "The effect of haptic interaction between balance assessment robot and pelvis on muscle activation of leg muscles," in *Proc. Int. Conf. Rehabil. Robot. (ICORR)*, Jul. 2017, pp. 234–239, doi: 10.1109/ICORR.2017.8009252.
[23] K.-R. Mun, Z. Guo, and H. Yu, "Development and evaluation of a novel overground robotic walker for pelvic motion support," in *Proc. IEEE Int. Conf. Rehabil. Robot. (ICORR)*, Aug. 2015, pp. 95–100, doi: 10.1109/ICORR.2015.7281182.
[24] A. Olenšek, M. Zadravec, and Z. Matjačić, "A novel robot for imposing perturbations during overground walking: Mechanism, control and normative stepping responses," *J. Neuroeng. Rehabil.*, vol. 13, no. 1, p. 55, Jun. 2016.
[25] K. O. Arras, S. Grzonka, M. Luber, and W. Burgard, "Efficient people tracking in laser range data using a multi-hypothesis leg-tracker with adaptive occlusion probabilities," in *Proc. IEEE Int. Conf. Robot. Automat.*, May 2008, pp. 1710–1715.
[26] W. Zijlstra and A. L. Hof, "Displacement of the pelvis during human walking: Experimental data and model predictions," *Gait Posture*, vol. 6, no. 3, pp. 249–262, Dec. 1997.
[27] M. W. Whittle and D. Levine, "Three-dimensional relationships between the movements of the pelvis and lumbar spine during normal gait," *Hum. Movement Sci.*, vol. 18, no. 5, pp. 681–692, Oct. 1999.

[28] T. Watanabe, E. Ohki, T. Ando, and M. G. Fujie, "Fundamental study of force control method for pelvis-supporting body weight support system," in *Proc. IEEE Int. Conf. Robot. Biomimetics*, Feb. 2009, pp. 1403–1408, doi: 10.1109/ROBIO.2009.4913206.
[29] G. Wang, J. Yan, and Y. Liu, "The spatial-temporal parameters and kinematics analysis of stroke hemiplegic gait," *Chin. J. Rehabil. Med.*, vol. 25, no. 12, pp. 1148–1151, Dec. 2010, doi: 10.3969/j.issn.1001-1242.2010.12.006.
[30] R. D. Seidler, Y. Kwak, B. W. Fling, and J. A. Bernard, "Neurocognitive mechanisms of error-based motor learning," *Adv. Exp. Med. Biol.*, vol. 782, pp. 39–60, Jan. 2013, doi: 10.1007/978-1-4614-5465-6_3.
[31] J. C. Ji, S. Guo, F. J. Xi, and L. Zhang, "Design and analysis of a smart rehabilitation walker with passive pelvic mechanism," *J. Mech. Robot.*, vol. 12, no. 3, Jan. 2020, Art. no. 031007.
[32] Z. Song, W. Chen, W. Wang, and G. Zhang, "Dynamic modeling and simulation of a body weight support system," *J. Healthcare Eng.*, vol. 2020, pp. 1–7, Feb. 2020.
[33] S. H. Kim and K. B. Reed, "Robot-assisted balance training for gait modification," in *Proc. IEEE 13th Int. Conf. Rehabil. Robot. (ICORR)*, Jun. 2013, pp. 1–4, doi: 10.1109/ICORR.2013.6650421.
[34] M. M. Wu, G. Brown, and K. E. Gordon, "Control of locomotor stability in stabilizing and destabilizing environments," *Gait Posture*, vol. 55, pp. 191–198, Jun. 2017.

JIANCHENG (CHARLES) JI (Student Member, IEEE) received the B.S. degree in mechanical engineering from Huazhong Agriculture University, Wuhan, in 2013, and the M.S. and Ph.D. degrees in mechanical engineering from Shanghai University, Shanghai, in 2016 and 2019, respectively.

He currently holds a postdoctoral position with Shenzhen Institutes of Advanced Technology, Shenzhen, China. His research interests include flexible multi-body dynamics, dynamic balance, and gait training with robotic devices for stroke patients and disabled elders. He was a recipient of the Honorable Mention for the 2020 *Journal of Mechanisms and Robotics* Best Paper Award, in 2021.

WEI CHEN was born in Jiamusi, Heilongjiang, China, in 1967. She received the Ph.D. degree in mechanical engineering from Harbin Institute of Technology, in 2000.

From 2000 to 2007, she was an Assistant Professor with Shenzhen Polytechnic. Since 2007, she has been a Professor with the Department of Mechanical Engineering, Shenzhen Polytechnic, where she has been working with the Intelligent Manufacturing Technology Research Institute, since 2008. Her research interests include mechanism and dynamics of robots. Her current research in robots focuses on the mechanism design and motion control of rehabilitation robot.

WENBIN WANG received the Ph.D. degree in mechanical manufacture and automation from Shanghai University, in 2007. He is currently working as an Associate Professor with Shenzhen Polytechnic. His research interests include image processing, soft robot, and industry robot and applications.

JASON XI received the B.M.Sc. degree from Schulich School of Medicine and Dentistry Honours Specialization Program in medical sciences. He is currently pursuing the M.Sc. degree with the Physical Therapy Program, Temerty Faculty of Medicine, University of Toronto. His current research interests include muscle anatomy for exercise and rehabilitation.